Stereoscopic Planar Laser-Induced Fluorescence Imaging at 500 kHz

T. L. Medford[*], P. M. Danehy[†], S. B. Jones[‡],
B. F. Bathel[§], J. A. Inman[**],
NASA Langley Research Center, Hampton, VA 23681-2199

N. Jiang[††], M. Webster[‡‡], W. Lempert[§§]
The Ohio State University, Columbus, OH 43210

J. Miller,[***] T. Meyer[†††]
Iowa State University, Ames, IA 50011

A new measurement technique for obtaining time- and spatially-resolved image sequences in hypersonic flows is developed. Nitric-oxide planar laser-induced fluorescence (NO PLIF) has previously been used to investigate transition from laminar to turbulent flow in hypersonic boundary layers using both planar and volumetric imaging capabilities. Low flow rates of NO were typically seeded into the flow, minimally perturbing the flow. The volumetric imaging was performed at a measurement rate of 10 Hz using a thick planar laser sheet that excited NO fluorescence. The fluorescence was captured by a pair of cameras having slightly different views of the flow. Subsequent stereoscopic reconstruction of these images allowed the three-dimensional flow structures to be viewed. In the current paper, this approach has been extended to 50,000 times higher repetition rates. A laser operating at 500 kHz excites the seeded NO molecules, and a camera, synchronized with the laser and fitted with a beam-splitting assembly, acquires two separate images of the flow. The resulting stereoscopic images provide three-dimensional flow visualizations at 500 kHz for the first time. The 200 ns exposure time in each frame is fast enough to freeze the flow while the 500 kHz repetition rate is fast enough to time-resolve changes in the flow being studied. This method is applied to visualize the evolving hypersonic flow structures that propagate downstream of a discrete protuberance attached to a flat plate. The technique was demonstrated in the NASA Langley Research Center's 31-Inch Mach 10 Air Tunnel facility. Different tunnel Reynolds number conditions, NO flow rates and two different cylindrical protuberance heights were investigated. The location of the onset of flow unsteadiness, an indicator of transition, was observed to move downstream during the tunnel runs, coinciding with an increase in the model temperature.

---

[*] NASA USRP Student, Advanced Sensing and Optical Measurements Branch, MS 493, and Undergraduate Student at Georgia Institute of Technology.
[†] Research Scientist, Advanced Sensing and Optical Measurement Branch, MS 493, AIAA Associate Fellow.
[‡] Technician, Advanced Sensing and Optical Measurement Branch, MS 493.
[§] PhD Student, University of Virginia, Charlottesville VA and Graduate Student at the National Institute of Aerospace, Hampton VA, AIAA Student Member.
[**] Research Scientist, Advanced Sensing and Optical Measurement Branch, MS 493, AIAA Member.
[††] Research Associate, AIAA Senior Member.
[‡‡] Graduate Research Assistant, AIAA Student Member.
[§§] Professor, AIAA Associate Fellow.
[***] Graduate Research Assistant, AIAA Student Member.
[†††] Assistant Professor, AIAA Associate Fellow.

I.   Introduction

Understanding and predicting transition from laminar to turbulent flow in hypersonic boundary layers is an active and important field of research because transitional and turbulent heating can be four or more times higher than laminar heating on hypersonic vehicles[1],[2] including the proposed Orion Crew Exploration Vehicle (CEV).[3] In hypersonic ground-test facilities, these transitional boundary layer flows are characterized by high speeds (1-3 km/s) and small (cm to mm) spatial scales that are accompanied by steep gradients in the flow properties. These factors drive the spatial resolution and frequency-response requirements of the instrumentation used to visualize and quantify these types of flows. For example, a flow structure with a 1-mm length scale travelling at a speed of 1 km/s can only be resolved using instrumentation with sub-mm spatial resolution and greater than 1 MHz frequency response. In ground test facilities, such structures can transit through a few-mm thick boundary layer having steep velocity gradients.   Thus, the instrumentation used should have a high spatial resolution in all three spatial dimensions.   Ideally, spatially-resolved volumetric data would be obtained at a fast sampling rate, with each individual measurement being temporally resolved (not averaged in time, relative to the time-scales in the flow). Similar challenges exist in other research fields such as explosions and detonations.

Several different measurement approaches have been developed to temporally resolve and acquire volumetric flow visualization or quantitative 3D data in both subsonic and supersonic flows. Approaches using scanning laser sheets,[4-16] tomography,[17-19] holography[20] and stereoscopic photography[21-23] have been demonstrated with some success but the spatial resolution typically gets worse as the sampling time is shortened. Reference 24 provides a detailed discussion of the relative merits and limitations of many of these volumetric imaging approaches. Reference 24 also introduces the stereoscopic nitric-oxide planar laser induced fluorescence (NO PLIF) technique, which provides high resolution volumetric flow visualizations with flow freezing (sub-microsecond) time integration.

With a few notable exceptions, most of these prior instruments acquired volumetric data at rates too slow to time resolve the flowfields being studied. References 5, 7, and 11 developed a three-dimensional imaging system that could obtain time-sequence data at a repetition rates of 20-50 Hz, which was fast enough to time resolve the low velocity (<3 m/s) water and air flows investigated. More recently, Schroeder et al.[19] developed a tomographic PIV system that could frame at 5 kHz while acquiring quantitative velocity measurements in a large flow volume. Such a system would be suitable for time-resolving flows with velocities of about a hundred meters per second, depending on the image resolution and size of the structures being investigated. However, such a system is still two orders of magnitude too slow to time-resolve the evolution of hypersonic boundary layer flows of interest here.

In the current paper, a MHz-rate NO PLIF system,[25],[26] is combined with the stereoscopic PLIF[24] technique to obtain time-sequence, volumetric flow visualizations for the first time. The system provides measurements with sub-mm spatial resolution, 200-ns time resolution in each image, and acquires data at a rate of 500 kHz. The volumetric information is provided by stereoscopic reconstruction of a pair of NO PLIF images acquired using a 5-mm thick laser sheet. The system is shown to be able to spatially and temporally resolve a transitional hypersonic boundary layer flow.

II.   Experiment and Analysis Description

The experiments were performed in the 31-Inch Mach 10 Air Tunnel at NASA Langley Research Center. The test apparatus consisted of three main components: the test article, the wind tunnel facility, and the MHz Stereoscopic PLIF system. The analysis used different image processing techniques to produce stereoscopic red/blue anaglyphs from the raw images. These apparatuses and procedures are summarized briefly in this section.

A. Test Article

The test article was a 20° full-angle wedge with a sharp leading edge. The wedge model is designed to hold different shape and size protuberances, also known as *trips*. Figure 1 shows computer renderings of the trip and the model. The top surface of the wedge is a planar surface, herein referred to as a *flat plate*. The flat plate is 127.0-mm (5-in.) wide and 162.5-mm (6.4-in.) long.

In the current experiment, two different protuberances were attached to this surface to trip the flow from laminar to turbulent. The two cylindrical protuberances used had the following dimensions: (1) 1.05±0.03-mm tall with a diameter of 4.08±0.03 mm, and (2) 2.05±0.03-mm tall with a diameter of 4.08±0.03 mm before being painted matte black. These are nominally referred to as 1- and 2-mm tall cylindrical trips, respectively. The edges of the trips were sharp. The center of each cylindrical trip was mounted 75.4±0.2 mm (2.97 in) downstream of the sharp leading edge of the model. References 27 and 28 describe the 11.0±0.1-mm wide seeding slot and various issues regarding the potential perturbations to the flow caused by the seeding system used to inject NO into the laminar boundary layer upstream of the trip.
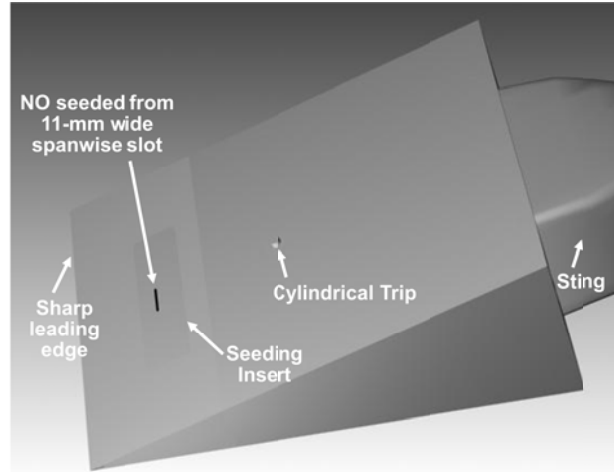

Figure 1. Test article used in the experiment, showing the assembled wedge model, seeding slot and cylindrical trip.

The model used in these experiments contained some imperfections. For the current test, Test 467, the imperfections were the same throughout all the runs. During this test, the seeding insert was slightly raised, resulting in forward and rearward facing steps of approximately 0.05 mm located upstream of the protuberance. Details can be obtained from the authors. These surface imperfections were approximately an order of magnitude smaller than the 1- and 2-mm tall trips used to perturb the flow in this experiment. To first order, the model imperfections described should be negligible, but could have an effect on higher fidelity computations of the flow.

B. Wind Tunnel, Tunnel Operating Conditions and Data Acquisition

The 31-Inch Mach 10 Air Tunnel is an electrically-heated blowdown facility located at the NASA Langley Research Center in Hampton, Virginia, USA. Reference 29 includes details of this facility of which a brief summary is provided here. The facility has a nominal Mach number of 10 and a 0.787 m (31 in.) square test section that operates with electrically heated, compressed air. Large windows, transparent in the ultraviolet, form three walls (including top and bottom) of the test section with the fourth wall formed by the model insertion system. In the experiments, the model was side-mounted to this fourth wall. Run durations for the current test were about 90 seconds. The nominal stagnation temperature was 1,000 K (1,340° F) for all tests. Two different facility stagnation pressures, P_0, were used: 4.96 MPa (720 psia) and 6.89 MPa (1000 psia). The two operating pressures simulate freestream unit Reynolds numbers of 3.3 and 4.6 million/m (1.0 and 1.4 million/ft), respectively. Table 1 summarizes the test conditions and configurations for the stereoscopic MHz data presented in this paper. Further details of the flow properties at these conditions can be found in Hollis et al.[30] or can be requested from the authors. The ratio of the trip height, k, to the boundary layer thickness, δ, and the roughness Reynolds number (Re_k), based on the trip height and the conditions at the trip height, were computed for each run as described in Reference 27.

Test	Run	Trip Type	Trip Height, k	Trip Width	Stagnation Pressure	Stagnation Temperature	Unit Reynolds Number	k/δ	Re_k	Plate Angle	NO flow rate
			(mm)	(mm)	(MPa)	(K)	(10^6/m)			(degrees)	(sccm)
467	21	cylinder	1	4	6.91	1003	4.58	1.2	4,140	20	300
467	23	cylinder	2	4	4.97	1003	3.34	2.1	5,960	20	300

Table 1. Experimental test cases reported in this paper.

The model was oriented so that the leading edge was vertical and facing the oncoming flow (which differs from the orientation shown in Fig. 1). The model was mounted to the far side wall of the tunnel with a strut mounted perpendicular to the wall and a sting mounted perpendicular to the strut so that the sting was initially aligned parallel to the freestream flow. The tunnel's yaw adjustment was then changed by +10°, resulting in a 20° angle between the

freestream flow and the flat plate. This angle, hereafter called the *plate angle,* was set to 20° for all the runs reported in this paper. An oblique shockwave originating from the leading edge of the model reduced the Mach number and velocity of the flow while increasing the gas static temperature and pressure. The post-shock Mach number was about 4, varying slightly with the operating conditions. The model was also rolled 1.5° counterclockwise (as viewed from downstream) so that the laser reflection from the tunnel's bottom window would not illuminate the flow field, instead hitting the side of the model, and thus not be visible to the camera. This slight roll angle should have a negligible effect on the fluid mechanics of the experiment.

C. MHz Planar Laser-Induced Fluorescence (PLIF) Imaging System

A custom built MHz-rate PLIF imaging system was used for this test. The laser is described in detail in Refs. 25 and 26 and is described briefly here. The laser system was installed next to the facility between the stairs and the blue instrument rack shown in Fig. 2. This laser produced bursts of pulses at a wavelength of 1.06 microns with about 100 mJ/pulse which is then converted to second (532 nm) and third (355 nm) harmonic wavelengths. The third harmonic (about 30 mJ/pulse) is then used as the pump for a custom-built injection-seeded optical parametric oscillator (OPO) system. The OPO output is sum-frequency mixed with residual 355 nm pump, creating 500 kHz, 20-pulse bursts of tunable output in the vicinity of 226 nm with about 0.15 mJ/pulse, which are used for the stereoscopic NO PLIF imaging. The repetition rate of the burst sequence is 1 Hz. The OPO "idler" beam is seeded by an External Cavity Diode Laser (ECDL), which results in line-narrowed output for both the idler and signal waves. The seeding laser was tuned to 823.9174 nm (vacuum wavelength), which after mixing with the third harmonic beam produced UV output at 226.1025 nm, exciting the $Q_1(12)+Q_{21}(12)$ and $Q_2(20)+Q_{12}(20)$ transitions of the NO A-X (0,0) band. Exiting the laser, the beam had a circular cross section with a 5 mm diameter. By the time it propagated 29 meters to the wind tunnel, the beam had diverged to a 20 mm diameter. The laser beam was then formed into a thick sheet using a combination of a cylindrical lens and a spherical lens. A positive 300 mm focal length cylindrical lens focused one axis of the beam which then propagated 1.2 meters and passed through a 1 meter focal length, 100-mm diameter spherical lens. This pair of lenses acted as a 3:1 telescope, increasing the width of the beam to 60 mm and collimating it in that axis. The spherical lens began to focus the beam in its other axis. However, the measurement location was not placed at the focus of the 1 meter lens. Rather it was placed 0.6 meters from the 1 meter focal length lens. The resulting laser sheet had a relatively constant rectangular cross sectional shape of 60 mm wide by 5 mm thick. The laser sheet was sufficiently thick to visualize the transitional flow structures, which typically stayed within 5 mm of the model surface based on prior measurements[28] at these, and similar, run conditions.
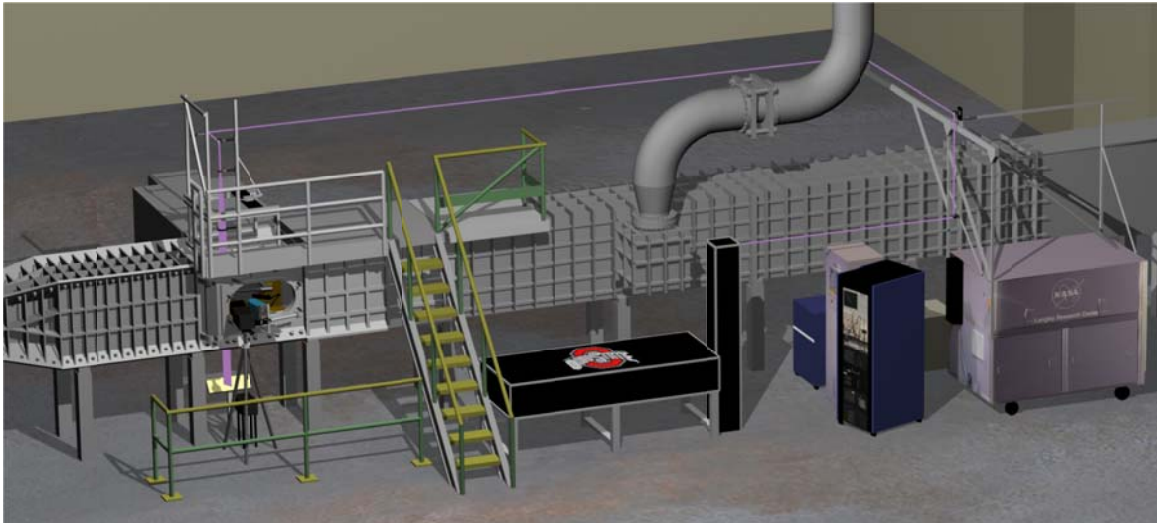

Figure 2. Schematic of the MHz NO PLIF systems installed adjacent to the 31-Inch Mach 10 Air Tunnel for Tests 467. The NASA 10 Hz NO PLIF system is shown on the far right side while the Ohio State University MHz NO PLIF system is shown immediately to the right of the stairs. The path of the laser beam is shown in light purple. The 10 Hz NASA NO PLIF system was not used in the current test.

PLIF image sequences were captured using a Princeton Scientific Instruments PSI-IV framing ICCD camera, equipped with a 100 mm F/2 UV lens from B. Halle GmbH. The PSI-IV image sensor consists of an 80 x 160 array of 115 x 115 micron pixels, each of which has its own integrated 28 element memory buffer, allowing 28 images to be obtained. Charge is shifted from the photo active area, which constitutes approximately 50% of the total pixel area, to memory at a maximum frame rate of 1 MHz. The camera used in this experiment consisted of a pair of sensors, with total available resolution of 160 x 160 pixels. A lens-coupled UV-sensitive micro-channel plate intensifier, with a fast decaying phosphor, was added in front of the camera to amplify the image intensity. The resulting magnification for this test was 2.54 pixels/mm (64.5 pixels/in) with a field of view equal to 63 mm x 63 mm (2.5 in x 2.5 in). Intensifier gains between 30% and 60% of the maximum were used for this experiment. The duration of the gate used to expose each individual frame was 200 ns, which is fast enough to freeze the flow: in 200 ns, gas travelling 1,000 m/s moves only 0.2 mm, which is less than the size of one pixel. The download time between image sequences was greater than 4 seconds, resulting in a 0.2 Hz repetition rate for the MHz laser/camera system to acquire bursts of pulses. Custom made transmission filters from Layertec, GmbH were placed in front of the camera lenses to efficiently block the laser's wavelength while transmitting most of the red-shifted fluorescence (transmit <1% @ 226nm and >80% @235-280nm).
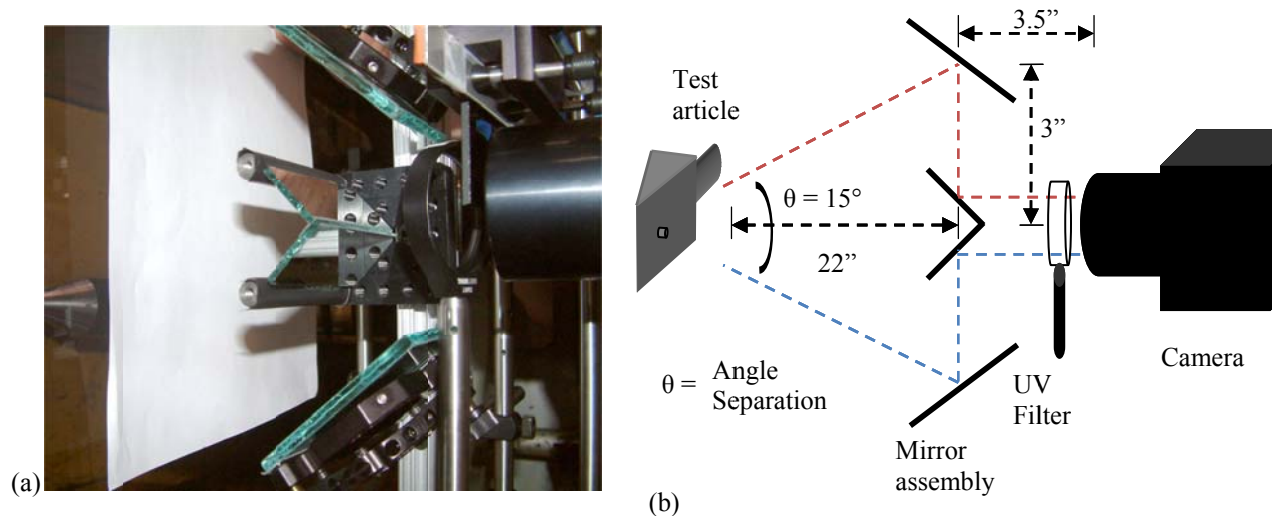

Figure 3. Photograph (a) shows the mirrored beam-splitter assembly used to divert the two different perspective views to the top and bottom CCDs of the camera. The camera is oriented in the vertical plane with the flow from left to right in the wind tunnel. A piece of white paper temporarily blocks the camera's view of the tunnel. The sting holding the test article is shown at the far left of (a). A circular UV filter can be seen placed in front of a 100mm fl, F/2 camera lens. Schematic (b) shows a dimensioned sketch of the PSI-IV MHz camera mirror assembly. The test article is drawn with the correct orientation but is not drawn to scale.

To obtain stereoscopic images, a mirror assembly was used to provide views of the flow from two different directions. The mirror assembly directed each view to the two separate, but adjacent, CCDs on the MHz camera. Each CCD recorded 10-20 sequential images to create a stereoscopic image set, with a two-microsecond time interval between each image, corresponding to a 500 kHz sampling rate. The mirror assembly, depicted in Fig. 3, consists of four mirrors located about 22 inches from the test article. An outer mirror separation distance of 6 inches creates a full-angle separation of 15 degrees, as shown by the colored dashed lines in the figure. Throughout the test, a camera saturation issue was observed with one of the camera's CCDs which degraded the image quality of one of the views. This is discussed in more detail below.

D. Stereoscopic PLIF Flow Visualization Image Processing

The raw grayscale stereoscopic PLIF image pairs were processed by subtracting a background (zero fluorescence signal) image from the image pairs. The images from the two CCDs on the camera were then separated into separate images, each containing a different perspective view of the same flow volume. Raw images were observed to have significant streaks caused by variations in the laser spatial energy distribution. An approximate method was used to correct for these spatial variations. This method assumes that the total amount of NO distributed spanwise across

each image is constant in the streamwise direction of the image. Thus, the main streamwise variations in the fluorescence intensity are attributed entirely to the laser energy. To correct for these energy variations, each (spanwise) row in the original image was binned into a single pixel, resulting in one column that corresponded to the averaged PLIF intensity at each streamwise location in the image. The original image pairs were then divided by this spatial energy distribution, resulting in smoother images that showed reduced laser-sheet intensity artifacts. A threshold was then applied to the images to reduce spurious noise. Finally, the stereoscopic image pairs were cropped where very low laser intensities occurred. The final step in processing the images prior to generating the red/blue anaglyphs was to increase the resolution of the images: the image pairs were scaled by a factor of two, interpolating to obtain the values of the new pixels, resulting in a pair of 160x320 images corresponding to each laser pulse.

E. Anaglyph Image and Movie Sequence Processing

The image pairs were then imported into the MATLAB®-based subroutine *anaglyph()* (version 2.0).[31] This subroutine combines the two grayscale images, obtained with different views, into a single image in which one view is colored red and the other view is colored blue, generating a so-called *anaglyph*. The subroutine was run in a loop to process multiple images to create movies or montages, as shown below. While several different methods[24] can be used to display stereoscopic image data, red/blue anaglyphs were chosen for this paper since they were the most accessible format to view the stereoscopic image sequences and movies and do not require specialized computer equipment. These images must be viewed through glasses having a red filter on the left eye and a blue filter on the right eye to produce the stereoscopic effect. The three-dimensional reconstructions occur in the viewer's brain as the right and left eyes see the two views from the stereoscopic anaglyph.

III.   Results

This paper displays stereoscopic data of runs with different Reynolds numbers, trip heights, and a varying amount of nitric oxide being seeded into the flow. Each run typically consisted of more than 20 image sequences totaling 400 images which maintained constant laser sheet positioning and/or model angle of attack. A few illustrative examples are selected from the runs to depict the features of the MHz stereoscopic NO PLIF visualization method.

A. Stereoscopic Flow Visualizations: Montage views

Figure 4 shows a montage of 8 time-correlated anaglyphs that were acquired with two-microsecond time spacing between images. The flow is from top to bottom in the images and the protuberance is near the top of each image. The laser sheet enters from the right side of the image, as evidenced by the shadow to the left of the protuberance in each image. The signal to noise ratio is the best in the middle and bottom of the images and is worse near the top of the images, where the laser intensity was lower. The individual flow structures can be seen and tracked as they progress and evolve downstream of the protuberance. The flow remains laminar, as evidenced by smooth, straight, streamwise streaks, for the first 12±2 mm downstream the cylindrical trip and then begins to develop into two helical, or corkscrew-shaped, structures that suggest vortical motion. Upon careful inspection, the two vortices, developing on the opposite sides of the trip appear to have opposite rotation and are often in phase with one another, as seen in Fig. 4(e). The vortex on the right side appears to rotate clockwise (as viewed from downstream) as it propagates downstream while the left-side vortex rotates in the opposite direction. These corkscrew-shaped vortices begin to break down into more irregular structures, suggestive of turbulence, as they propagate downstream.
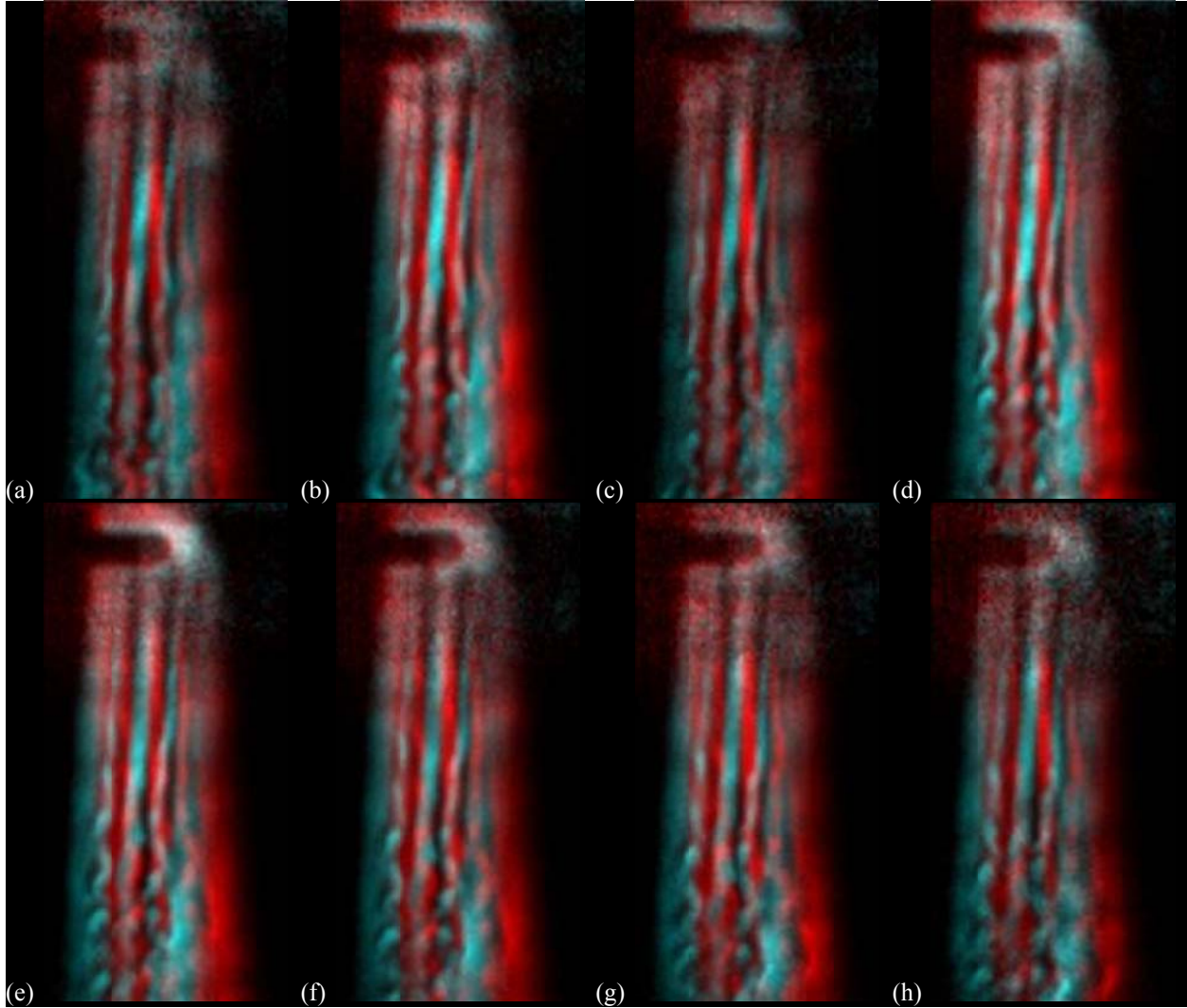
Figure 4. Test 467, Run 21: Eight sequential MHz NO PLIF anaglyphs for flow over a 1-mm tall by 4-mm wide cylinder with a seeded NO flow of 300 sccm, $P_0 = 6.91$ MPa. The images were acquired consecutively at a rate of 500 kHz. Flow is from top to bottom. Each image measures 56 mm from top to bottom.

The roughness Reynolds number, Re_k evaluated based on the conditions at the trip height, k, is a parameter that is sometimes used to correlate the transition from laminar to turbulent flow in tripped hypersonic boundary layers (see Reference 32 for a recent review). Flows with higher values of Re_k are more likely to transition to turbulence. By using a trip two times larger, the Re_k was increased by nearly a factor of 1.5 between Runs 21 and 23 as shown in Table 1. The Re_k increased despite the fact that the tunnel stagnation pressure, P_0, and unit Reynolds number of the tunnel had decreased from the previous run. Another common scaling parameter is the ratio of the trip height to the boundary layer thickness, k/δ, with increasing k/δ corresponding to an earlier onset of transition.[32] Between Runs 21 and 23, k/δ increased by a factor of 1.75, as showing in Table 1. As expected based on the increases in Re_k and k/δ, the images from Run 23, shown in Fig. 5, show much shorter induction length before the laminar structures transition to irregular structures. Corkscrew shaped vortices now appear to form adjacent to the right side of the trip. Again, the corkscrew-shaped structure appears to rotate counterclockwise as viewed from downstream, as in Fig. 4, and propagates downstream where it devolves into smaller more irregular flow structures. Other measurements occurring in the same run behaved similarly. Measurements were also performed at lower stagnation pressure

The American Institute of Aeronautics and Astronautics

conditions, and as expected, these appeared more laminar. However, the signal-to-noise ratio was worse in those images, owing to the camera problems detailed below, so these results are not presented herein.
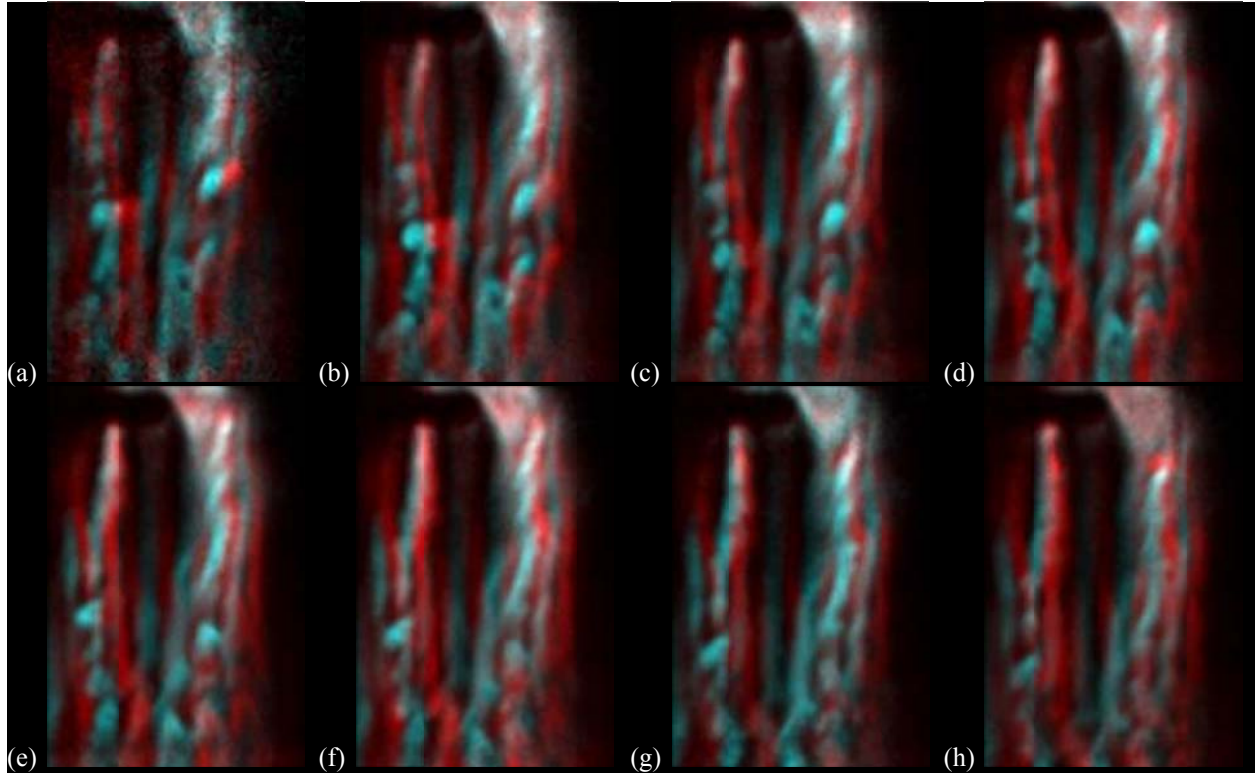

Figure 5. Test 467, Run 23: Eight sequential MHz NO PLIF anaglyphs for flow over a 2-mm tall by 4-mm wide cylinder with a seeded NO flow of 300 sccm, P_0 = 4.96 MPa. The images were acquired consecutively at a rate of 500 kHz. Flow is from top to bottom. Each image measures 41 mm from top to bottom.

Figure 6 shows a much higher nitric-oxide seeding rate at the end of the same run as in Fig. 5. The more than ten times increase in flow rate of NO itself trips the flow to transition towards turbulence even before the location of the trip. The irregular structures are observed to propagate downstream while mostly maintaining their shape. Finer flow length scales are observed at the downstream (bottom) end of the images in Fig. 6. Comparing Figs. 5 and 6, the observed flow structures are significantly different, suggesting that either different transition mechanisms are occurring or that the flow in Fig. 6 has just progressed further towards transition.
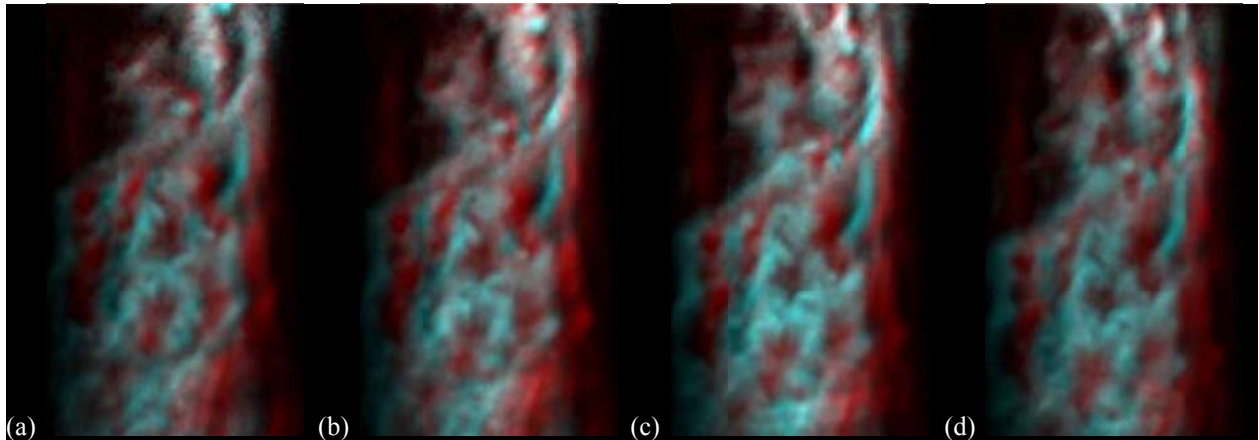
The American Institute of Aeronautics and Astronautics

(a)   (b)   (c)   (d)

Figure 6. Test 467, end of Run 23: Four sequential high-NO-flow rate MHz NO PLIF anaglyphs for flow over a 2-mm tall by 4-mm wide cylinder,, P_0 = 4.96 MPa. The images were acquired consecutively at a rate of 500 kHz. Flow is from top to bottom. Each image measures 46 mm from top to bottom. The camera 30% gain used to obtain these images was half that used to acquire the data in Fig. 5.

B. 500 kHz Stereo PLIF Video

By combining the anaglyph images from a single time-correlated laser pulse burst, NO PLIF anaglyph movies were created. These movies more clearly (than the montages shown above) allow the time-evolution of the three dimensional flow structures to be observed as they propagate and evolve downstream. Figure 7 shows the anaglyph image set from Fig. 4 which were used to create slow-motion visualizations of the propagating flow structures. From Fig. 7, the progression of the flow features can be seen as they travel downstream of the flow disturbance displaying the counter rotating vortices and/or breaking apart into smaller flow structures.

C. Effect of Model Heating

During most of the runs, which lasted about 90 seconds, the laser sheet position and all other test variables were held constant to allow for multiple sequences of images to be taken at the same conditions. The only parameter that changed significantly during the runs was the temperature of the flat plate model, which increased due to heating by the T_0 = 1000 K oncoming flow. From Fig. 8, it can be seen that the flow structures tend to change to more laminar flow as the run proceeds. That is, the length of the steady, straight, laminar flow region increases with run duration. While the transition process is stochastic and some image-sequence-to-image-sequence variations in laminar induction length were observed, the general trend during the runs was towards more laminar flow as the run progressed. As a specific example, in Fig. 8, at 56 sec, the position at which instabilities the size of the trip width (4 mm) occur is more than twice as far downstream compared to earlier in the run, at 11 sec. It is speculated that model heating is the source of the changes in the observed images. A higher surface temperature would decrease the density of the gas in the boundary layer, thereby

Figure 7. MHz NO PLIF anaglyph movie sequence.

slightly increasing the boundary layer thickness, δ, reducing k/δ during the run and decreasing the tendency towards transition. Such model heating effects must be taken into account in future experiments and computations if direct comparisons are to be made. In general, the heating of the wall would also cause the Reynolds number to decrease, because the gas density decreases while the dynamic viscosity increases. Such a decrease in Reynolds number would delay transition onset as the run progressed. However, since the parameter Re_k is evaluated at the trip height, and since the trip is larger than the thickness of the boundary layer, Re_k actually stays constant as the model heats up during a run. Reference 32 discusses the applicability of Re_k as a correlation parameter if $k > \delta$.
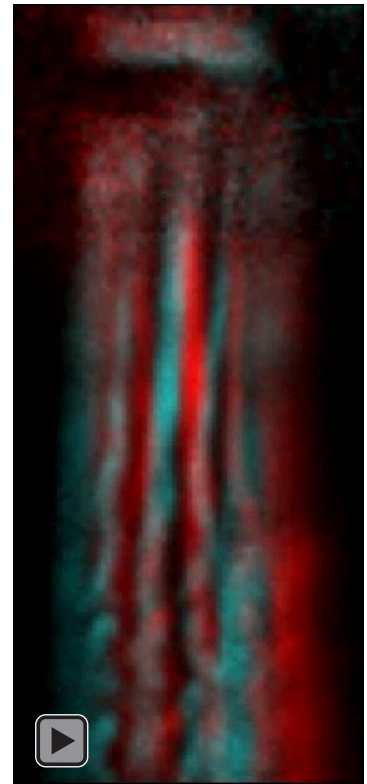
9

The American Institute of Aeronautics and Astronautics
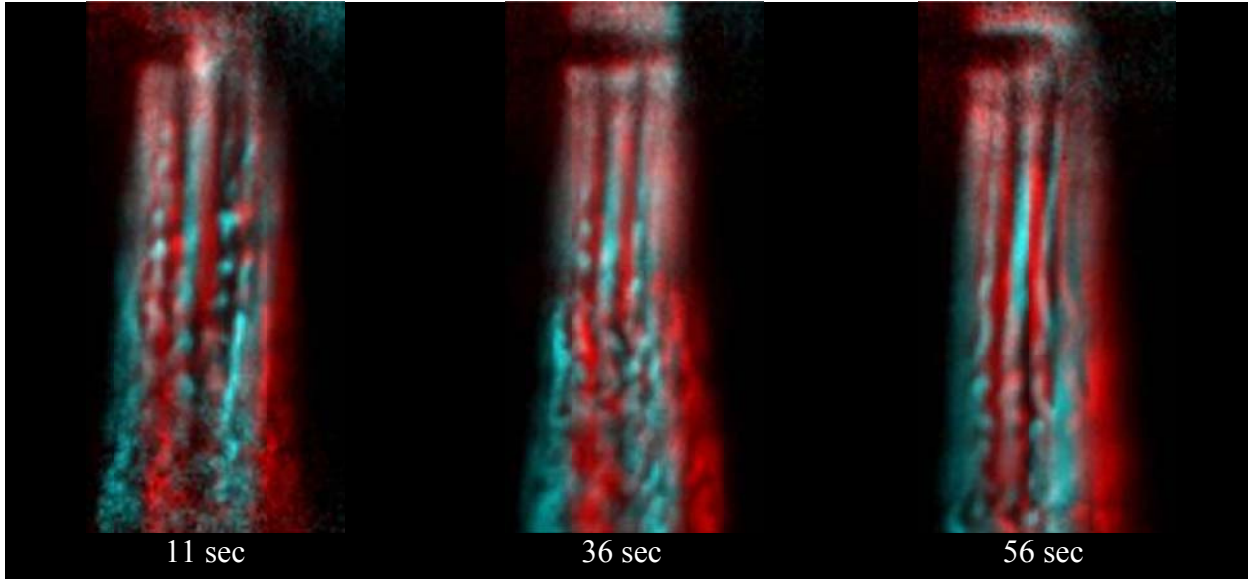
| 11 sec | 36 sec | 56 sec |

Figure 8. Test 467, Run 21: Three uncorrelated MHz NO PLIF anaglyphs for flow over a 1-mm tall by 4-mm wide cylinder with a seeded NO flow of 300 sccm, P_0 = 6.91 MPa. Flow is from top to bottom. Images are taken from beginning, middle, and end of the run.

In the current tests, the surface temperature of the flat plate was not monitored. However, in a past test (Test 443) in runs that operated at the same and/or similar conditions, a thermocouple was attached to back side of the 0.2 inch thick stainless steel flat plate. The thermocouple was attached near the location of the trip. While not a direct measure of the front-surface temperature, the measurement provides an indication of the flat plate's starting surface temperature and the rate of change in temperature during the run. These prior runs were obtained in the same facility with the same model, the same angle of attack, and the same trip geometry. The back-side flat plate temperature was observed to stay constant for the first 5-7 seconds of the run, during which heat is being conducted through the plate but has not yet reached the thermocouple. The thermocouple then smoothly transitions to a steadily increasing temperature. The rate of temperature increase is constant between 20 and 60 seconds in the run. Based on the data obtained in Test 443, the magnitude of this rate increases linearly with the stagnation pressure, allowing the rate of temperature increase ($\Delta T/\Delta t$) to be estimated for intermediate pressures not tested with the thermocouple. It was also observed that the model temperature started at about 30 °C when the run was the first of the day, while it started at 50 °C when another run took place an hour earlier. To estimate the temperature at the surface of the model during the runs in Test 467, it was further assumed that the surface temperature started increasing immediately when the model was injected into the wind tunnel, thereby removing the delay caused by heat conduction through the plate in the measurements. Based on these assumptions and the knowledge of the likely temperature of the model at the start of the run, the surface temperature was estimated, with the results shown in Table 2. The initial temperatures are estimated to be accurate to within ±5 °C while $\Delta T/\Delta t$ is estimated to be accurate within 10%, based on data from repeated runs in Test 443.

In Table 2, surface temperature increases of 50 °C are estimated to occur during the first minute of the run. Runs lasted up to 90 seconds, which would result in estimated temperature increases as large as 72 °C, potentially having significant effects on the boundary layer thickness and Reynolds number.

Run	T_{start}	$\Delta T/\Delta t$	$T_{60\ sec}$
	(°C)	(°C/sec)	(°C)
Run 21	50	0.80	98
Run 23	50	0.67	90

Table 2. Estimated starting surface temperatures and temperature increase during the runs, at the location of the trip, based on thermocouple data obtained in Test 443. T_{start} is the estimated temperature at the start of the run while $T_{60\ sec}$ is the estimated temperature 60 seconds into the run

IV.   Discussion

The stereoscopic MHz NO PLIF system demonstrates the ability to freeze the motion and visualize 3-dimensional flow structures of hypersonic flows in a manner previously demonstrated with a 10-Hz NO PLIF system.[24] However, use of the MHz system allows repeated observations with microsecond-scale time increments that allow changes in the flow structures and propagating flow field to be monitored.

Compared to stereoscopic images acquired with the 10 Hz NO PLIF system,[24] the current images have a weaker stereoscopic effect. There are several possible reasons for this. First, the 10 Hz system used a pair of cameras, each having 512x512 pixels whereas the CCD's used in the current experiment had 80x160 pixels, roughly 5x lower resolution in each dimension. The more spatial information present in the images, the easier for the brain to interpret the images and assimilate them. Second, the 15 degree angular separation between the two views in the current experiment is slightly larger than the 12 degree separation used in the 10-Hz experiment. These large angular separations were used to enhance the three-dimensionality of the thin boundary layer structures, but, generally speaking, the wider the angular separation of the camera views, the more difficult it is for the brain to reconstruct the views since they look less natural. Third, and most important, the signal-to-noise ratio was worse in the current data set than in the prior 10-Hz experiment.

Low signal-to-noise ratio in PLIF experiments often occurs because of one or more of the following reasons: (i) too low laser intensity (ii) too few camera counts, (iii) too high camera gain used, (iv) too small-aperture (high f-number) collection optics or (v) not enough seed species (nitric oxide in the current experiment). None of these were the cause of the low signal-to-noise ratio in the current experiment. High signal-to-noise ratio images with 6,000-8,000 counts (out of 16,000) could be obtained on one of the camera's CCD sensors with intensifier gains set to 50-80% of the maximum with the level of laser intensity available and amount of NO seeding used. Intensifier gains up to 80% did not result in excessively noisy images. The other, identical, CCD sensor showed an anomalous saturation behavior when the signal intensity exceeded approximately 1000 to 1500 counts above background. This CCD appeared to be damaged. Consequently, lower intensifier gains (30-50%) were required to prevent saturating this sensor. To make matters worse, images having signals below 300-500 counts above background appeared to be noisy owing to the camera's thermal noise. Thus, only signal intensities in the small range of about 1000 counts would produce images that were both above the background noise and below the saturation limit. Unfortunately the pulse-to-pulse energy of the pulse burst laser varies by a factor of 2-3 burst to burst. There can also be up to a factor of 2 variation in pulse energy within a burst. At a repetition rate of 0.2 Hz, only 15 image sequences could be obtained per 90 sec. tunnel run. Few of these image sequences resulted in images that were above the noise level of the CCD while being below the saturation level of the damaged CCD. Even in the best image sequences, evidence of the saturation problem can be observed, for example in Fig. 5 in which the red images appear to be more washed out than the blue images, particularly in the lower half of the images. If this high-speed imaging technique is applied using a camera system not having this saturation issue, many more, higher quality, stereoscopic visualizations could be obtained. The system could also be significantly improved by using a higher-resolution camera.

Some advantages of this volumetric imaging are that the resolution of the imaging system is determined by the camera used; in this case 160 x 160 pixels, and that the setup differs little from conventional thin-laser-sheet PLIF imaging in that only slight modification to the sheet forming optics and the camera system are needed. However compared to other three dimensional flow visualization systems, this technique does have a major disadvantage: it is difficult, though not impossible, to extract point-by-point three dimensional spatial information from the image pairs.[21] In addition, the flow must also be seeded with a tracer gas or must have a fluorescent species present in the flow.

The 500 kHz stereoscopic PLIF capability demonstrated herein could easily be extended to increase the speed by a factor of 2 (to 1 MHz) by simply triggering the laser and camera at 1 MHz as in past work.[26] However, the performance of the laser is worse under these conditions: a factor of 2 fewer pulses are obtained from the laser, resulting in a factor of 4 reduction in the overall duration of observation (e.g., 6 μsec vs. 24 μsec). The hypersonic flow structures studied thus far with this method do not appear to change appreciably on time scales of 1-2 μsec, so use of the system at 500 kHz is advised. The system can also be slowed down to operate at 100 kHz or even 10 kHz for lower-speed applications. At the lower repetition rates, higher-resolution camera technology exists that could be employed to increase the spatial resolution. Also, at the lower repetition rates the laser can produce many more pulses per burst (for example 100 pulses at 100 kHz), so longer movie sequences can be obtained; lower frequency

cameras can acquire longer movie sequences as well. The technique could be applied to image other species besides nitric oxide. For example, imaging the hydroxyl radical (OH) in the same fashion would provide useful three-dimensional views of combustion radicals in high-speed combustion flows such as scramjet engines.

V.   Conclusion

A stereoscopic NO PLIF system operating at 500 kHz, visualized three-dimensional flow structures in a transitional hypersonic boundary layer. The technique temporally resolved unsteady flow structures as they propagated downstream of cylindrical protuberances. This new visualization technique may help improve understanding of hypersonic flows and could be useful in other applications where visualization of unsteady, high-speed flows is needed, such as detonations, supersonic combustion systems and explosions.

This method has sub-mm spatial resolution and sub-microsecond time resolution capable of visualizing hypersonic flows with flow-freezing time response. The 2 µsec interframe time allows the flows to propagate a few pixels between images, allowing the development and evolution of the flow structures to be observed. The three-dimensional information provided by the technique offers a more complete visualization of the flow compared to the thin laser sheet NO PLIF method or the 10 Hz stereoscopic NO PLIF method. However, in their current form, the stereoscopic data are less spatially precise than a thin-sheet scanning approach. Compared to conventional thin-laser-sheet imaging methods where all three spatial coordinates are known for each image, the stereoscopic images are somewhat harder to interpret. Furthermore, the image quality is significantly worse than the 10 Hz stereoscopic method, owing to the lower pixels resolution and a saturation issue with the MHz-rate camera system. Nonetheless, the 500 kHz rate stereoscopic imaging system presented here demonstrates a 50,000 times increase in repetition compared to prior 3D visualization systems, which allows time-sequence images of the flow to be obtained.

Acknowledgments

References

[1] R. L. Wright, E. V. Zoby, "Flight measurements of boundary-layer transition on a 5 deg half-angle cone at a free-stream Mach number of 20 (reentry F)," Rept Number: L-7506; NASA-TM-X-2253 May 1 1971.

[2] S. A. Berry and T. J. Horvath "Discrete-Roughness Transition for Hypersonic Flight Vehicles," J of Spacecraft and Rockets Vol. 45, No. 2, March–April 2008.

[3] S. Berry, T. Horvath, R. Lillard, B. Kirk, A. Cassady "Aerothermal Testing for Project Orion Crew Exploration Vehicle," AIAA Paper 2009-3842, 41st AIAA Thermophysics Conference, San Antonio, Texas, June 22-25, 2009

[4] G. Kychakoff, P. H. Paul, I. Van Cruyningen, and R. K. Hanson, "Movies and 3-D Images of Flowfields Using Planar Laser-Induced Fluorescence," App. Optics, Vol. 26, pp. 2498-2500, 1987.

[5] M. Yoda and L. Hesselink, "A three-dimensional visualization technique applied to flow around a delta wing Experiments in Fluids 10, p.102-108 1990.

[6] W. J. A. Dahm, K. B. Southerland, and K. A. Buch Direct, high resolution, four-dimensional measurements of the fine scale structure of SC>> 1 molecular mixing in turbulent flows , Phys. Fluids A 3 (5), May 1991, p. 1115-1127.

[7] C. L. Delo, R. M. Kelso, and A. J. Smits, "Three-dimensional structure of a low-Reynolds-number turbulent boundary layer" Journal of Fluid Mechanics, 512:47-83, 2004.

[8] B. Yip, R. L. Schmitt, and M. B. Long, "Instantaneous three-dimensional concentration measurements in turbulent jets and flames," Opt. Lett. **13**, 96-99, 1988.

[9] B. J. Patrie, J. M. Seitzman, and R. K. Hanson, "Instantaneous Three-Dimensional Flow Visualization by Rapid Acquisition of Multiple Planar Flow Images," Opt. Eng., vol. 33, pp. 975-980, 1994.

[10] F. Ossler, S. Agrup and M. Alden "Three-dimensional flow visualization with picosecond Mie scattering and streak-camera detection" Applied Optics Vol. 34, No. 3 , pp. 537-540, 20 January 1995.

[11] J. E. Goldstein and A. J. Smits, "Flow Visualization of the Three-Dimensional, Time-Evolving Structure of a Turbulent Boundary Layer," Phys. Fluids, Vol. 6, pp. 577-587, 1994.

[12] T. C. Island, B. J. Patrie, M. G. Mungal, and R. K.. Hanson, "Instantaneous Three-Dimensional Flow Visualization of a Supersonic Mixing Layer," Exp. Fluids, Vol. 20, pp. 249-256, 1996.

[13] J. Hult, A. Omrane, J. Nygren, C. F. Kaminski, B. Axelsson, R. Collin, P.-E. Bengtsson, and M. Alden, "Quantitative Three-Dimensional Imaging of Soot Volume Fraction in Turbulent Non-Premixed Flames," Exp. Fluids, Vol. 33, pp. 265-69, 2002.

[14] B. S. Thurow, "Recent Progress Towards a High-Speed Three-Dimensional Flow Visualization Technique", 22nd International Congress on Instrumentation in Aerospace Simulation Facilities, Pacific Grove, CA, June 10 – 14th, 2007.

[15] B. Thurow, and K. Lynch, "Development of a High Speed Three Dimensional Flow Visualization Technique," AIAA Journal, Vol 47, pp. 2857-2865, 2009.

[16] S. Williams, M. Melnick, B. Thurow, "3-D Visualization of a Turbulent Boundary Layer." AIAA Paper 2010-4277, 40th AIAA Fluid Dynamics Conference, Chicago Illinois, June 2010.

[17] E.D. Torniainen, A. Hinz, and F. C. Gouldin, "Tomographic Analysis of Unsteady Reacting Flows," AIAA Journal, vol. 36, p. 1270-1278, 1998.

[18] C. J. Elkins, M. Markl, N. Pelc, and J. K. Eaton, "4D Magnetic resonance velocimetry for mean velocity measurements in complex turbulent flows," Exp. Fluids, Vol. 34, pp. 494-503, 2003.

[19] A. Schroeder, R. Geisler, G. E. Elsinga, F. Scarano, U. Dierksheide "Investigation of a turbulent spot and a tripped turbulent boundary layer flow using time-resolved tomographic PIV," Exp Fluids v. 44, p. 305–316, 2008.

[20] R. Snyder and L. Hesselink "Measurement of mixing fluid flows with optical tomography" Optics Letters, Vol. 13, No. 2, 87-89, February, 1988.

[21] W. B. Ng, Y. Zhang "Stereoscopic imaging and reconstruction of the 3D geometry of flame surfaces," Experiments in Fluids, Springer Berlin / Heidelberg , Vol. 34, No. 4, pp. 484-493, April, 2003.

[22] W.B. Ng, K.J. Syed and Y. Zhang, "The study of flame dynamics and structures in an industrial-scale gas turbine combustor using digital data processing and computer vision techniques," Experimental Thermal and Fluid Science Volume 29, Issue 6, pp. 715-723, July, 2005.

[23] K. Y. Cheung and Y. Zhang "Stereo imaging and analysis of combustion process in a gas turbine combustor" Meas. Sci. Technol. V. 17, pp. 3221-3228, 2006.

[24] P. M. Danehy, J. A. Inman, B. Bathel, D. W. Alderfer, S. B. Jones, "Stereoscopic Imaging in Hypersonics Flows using Planar Laser Induced Fluorescence", Paper Number 2008-4267, 26th AIAA Aerodynamic Measurement Technology and Ground Testing Conference, Seattle, WA June 23-26, 2008.

[25] N. Jiang, and W. Lempert, "Ultra-high frame rate Nitric Oxide Planar Laser Induced Fluorescence imaging", Optics Letters, 33, (19), 2236-2238, 2008.

[26] N. Jiang, M. Webster, W. R. Lempert, J. D. Miller, T. R. Meyer, C. B. Ivey, and P. M. Danehy, "MHz-rate nitric oxide planar laser-induced fluorescence imaging in a Mach 10 hypersonic wind tunnel," Applied Optics, Vol. 50, No. 4, Feb. (2011)..

[27] P.M. Danehy, C. B. Ivey, J.A. Inman, B. Bathel, S.B. Jones, A. C. McCrea, N. Jiang, M. Webster, W. Lempert, J. Miller, T. Meyer "High-speed PLIF imaging of hypersonic transition over discrete cylindrical roughness," Paper AIAA-2010-0703, the 48th AIAA Aerospace Sciences Meeting, Fluid Dynamics TC, Orlando Florida, January 2010.

[28] P. M. Danehy, B. Bathel, C. Ivey, J. A. Inman, S. B. Jones, "NO PLIF study of hypersonic transition over a discrete hemispherical roughness element", AIAA-2009-0394, 47th AIAA Aerospace Sciences Meeting, Orlando, FL, January, 2009.

[29] J. R. Micol "Langley Aerothermodynamic Facilities Complex: Enhancements and Testing Capabilities," AIAA Paper 98-0147, 36th AIAA Aerospace Sciences Meeting & Exhibit, January 12-15, Reno, NV, 1998.

[30] Hollis, B.R. "Real-gas flow properties for NASA Langley Research Center Aerothermodynamics Facilities Complex Wind Tunnels," NASA Contractor Report 4755, Sept. 1996.

[31] http://www.mathworks.com/matlabcentral/fileexchange/4977-anaglyph-ver-2-0

[32] S. Schneider, "Effects of Roughness on Hypersonic Boundary-Layer Transition " Journal of Spacecraft and Rockets, v.45 n.2 p.193-209, 2008